FEASIBILITY STUDY ON THE USE OF A WATER-COOLED SHELL AND TUBE HEAT EXCHANGER FOR A SCO_2 BRAYTON RECOMPRESSION CYCLE IN CSP APPLICATIONS

Mubenga C. Tshamala[1], **Michael Owen**[2], **Craig McGregor**[3], **and Zinhle Dlamini**[4]

[1] Stellenbosch University, Mechanical and Mechatronic Department, Joubert Street, Private Bag X1, Matieland 7602, South Africa; Phone: + 27 21 808 4243; E-mail: mctshamala@sun.ac.za

[2] Stellenbosch University; E-mail: mikeowen@sun.ac.za; [3] Stellenbosch University; E-mail: craigm@sun.ac.za

[4] Stellenbosch University; E-mail: zdlamini00666@gmail.com

Abstract: The Rankine cycle has been a leading power generation cycle for years. Recently however, the Brayton cycle, specifically the recompression configuration, has proven to be more efficient when using sCO_2. Studies have demonstrated that if the compressor inlet temperature and pressure of sCO_2 are maintained near the critical values, the cycle's efficiency can be improved. For this project, the goal was to design a water-cooled shell and tube heat exchanger (STHE) that can cool sCO_2 to within a range of 30°C to 33°C for a Brayton recompression cycle and evaluate its performance when used with CSP. The STHE was designed iteratively using the Bell Delaware method and TEMA standards. With FLOWNEX, a simulation of the Brayton recompression cycle with an inventory control system was conducted using DNI collected in the Upington area on the hottest day of the year. For this simulation, it was found that a minimum heat input of 35MW was required for accurate results. It was shown that even when the dew point temperature varies, the heat exchanger can maintain the required outlet temperature. However, it transpired that this could not result in the predicted 51.5% efficiency, but cycle temperatures revealed to be stable even during transient operation. To achieve the above efficiency, a combination of pressure ratio, split ratio, and main compressor inlet temperature (CIT) to the recommended range is required to ensure efficiency increase.

Keywords: Supercritical carbon dioxide Brayton cycle; Compact heat exchangers; Recompression cycles; Concentrated Solar Power.

1. Introduction

According to the International Energy Agency [1], the world energy demand is expected to continue its rise for the foreseeable future. The Stated Policies Scenario (STEPS) predicted an annual growth of 1% between 2022 and 2030, while the Announced Pledges Scenario (APS) predicted a 0.2% annual growth. However, it is necessary to highlight that these predictions account for the current energy crisis, leading to a 3.3% drop from the previous 2030 predicted GDP. In the South African context, about 80% of carbon emission derives from the energy sector, of which 50% is from electricity generation [2]. In-light of the above, there is a drive to further develop alternative sources of energy to feed the power generation industry to adequately respond to challenges of energy demand growth, high prices as well as the reduction of emissions. As such, in the search for alternative solutions, the Department of Mineral Resources and Energy of South Africa has embarked on a journey to diversify the energy supply for 2030 and beyond [2]. For instance, one of South African most attractive regions, the Upington region, with a recorded long-term annual average of 2816 kWh/m^2 of Direct Normal Irradiance (DNI) and 2282 kWh/m^2 of Global Horizontal Irradiance (GHI); is an under-utilized energy source that could potentially alleviate the strain on existing power plants because the area is exposed to relatively high solar irradiation that can greatly contribute to the power generation sector.[3]

However, these regions are often characterized by a combination very little to no rain, which results in water shortages, and very high ambient temperatures. It is recorded that the annual average rain can be as little as 83.3 mm and ambient temperatures, reaching maximum of 45.3°C between 1991 – 2020 [4]. The above constitutes a significant challenge when it comes to the design of effective heat rejection units for thermal power plants. The traditional steam Rankine cycle has been used for many years in thermal power generation for its ability to produce power at high efficiencies. In recent years, however, variations of the Brayton cycle are under investigation as they have shown potential for achieving competitive efficiencies, when operated using supercritical carbon dioxide (sCO_2) as working fluid [5]. The density of sCO_2 near the critical state resembles that of a liquid. Thus, the use of sCO_2 in a Brayton cycle offers reduced compression power and increases the cycle's overall efficiency [6]. In the early 2000s Dostal [7] investigated different sCO_2 cycle layouts to discover that the recompression layout is the most efficient layout of all.

To further improve the performance of the sCO_2 Brayton recompression cycle (BRC), it is important to analyse how the individual components can affect the overall efficiency. While there is much research on all the other power block components, there is unfortunately very limited research on heat rejection system design, as well as the impact of this system on the cycle's overall performance. Most plants attempt to avoid operating near the critical point of sCO_2 because the carbon dioxide thermo-physical properties are very sensitive to change in temperature or pressure is unstable in this region [8]. Specifically, there are rapid fluctuations in the fluid properties that affect the compressor performance. A 2℃ difference in the main compressor inlet temperature (CIT) can result in a 10% drop of adiabatic efficiency of the compressor [9]. Despite of the above, Ehsan [10] showed that if the CIT can be 35℃ or below, a BRC could operate at efficiencies higher than 49%. Attaining such lower temperature after the heat rejection unit in regions characterized by high ambient temperature as discussed earlier present many challenges; hence, it was recommended to investigate multiple cooling system designs to ensure delivery of CIT of below 35°C. Hence, for this study, a shell-and-tube heat exchanger (STHE) was identified as a suitable candidate due to its compactness, affordability, ability to sustain high pressure ranges and wide range of operating temperatures [11].

2. Aim

The objective of this study is thus to investigate the dynamic response of a water-cooled sCO_2 BRC for concentrated solar power (CSP) applications to simultaneous variations of solar resource, direct normal irradiation (DNI), and ambient temperatures. A previous study by Tshamala *et al.* [12], considered a concentrated solar powered sCO_2 BRC fitted with inventory control system, subjected to daily variation of DNI. The above cycle was simulated to predict the required cooling capacity of the heat rejection unit that would maintain the CIT constant at 35°C. The inventory control, however, was introduced to regulate and maintain the turbine inlet temperature (TIT) through cycle's mass flow rate control. Whilst the above study assumed a hypothetical heat rejection unit, in this study, a water-cooled shell-and-tube heat exchanger (STHE) is designed and integrated to the 1-D Flownex simulation model of the sCO_2 BRC and daily ambient temperatures are used as input to the STHE. This STHE is designed to deliver a CIT ranging between 30 – 33°C, aiming at improving the power block overall efficiency. It is essential to highlight that since the study of the turbomachinery is not part of the current scope, the built 1-D model simulation model used centrifugal pumps in place of compressors; this was decided in anticipation that in the transcritical region the fluid exhibits liquid-like properties, especially as its temperature continues decrease [13]. Simulation of the complete power block is performed to determine the overall cycle dynamic response and performance assessment is presented. However, the current investigation assumes that the cooling water is provided at ambient wet-bulb temperature in the Upington. The designed STHE will be used in ongoing research which will consider performance assessment of dry, wet and hybrid systems in an indirect cooling configuration.

3. sCO_2 BRC cooling method and design.

3.1. Brayton Recompression Cycle description

The original BC (Fig. 1) comprised three primary components. The compressor, combustion chamber and the turbine. Atmospheric air (State 1) would enter the compressor and be pressured to state 2 and then heated to state 3 to increase its specific volume to ensure greater power output in the turbine where it is expanded to state 4. After the turbine the exhaust gas is released into the atmosphere [6]. This is a very basic form of the BC when compared to the Brayton recompression cycle (BRC) (Fig. 2) which comprises two compressors, two recuperators, a turbine, a heater, and a cooler. The working fluid enters the main compressor (MC) at state 1 where the fluid is pressurised to state 2. The fluid is then heated in the low temperature recuperator (LTR) (2 – 3), as well as the high temperature recuperator (HTR) (4 – 5) using heat from the hot exhaust gases.

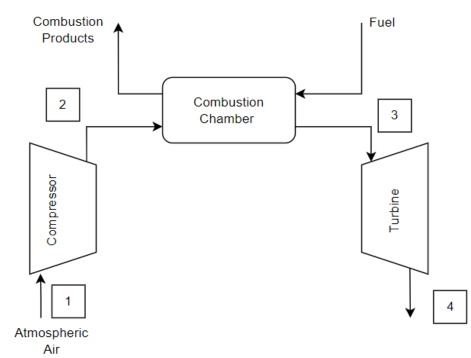

Fig. 1. Original Brayton Cycle Layout

Additional heat is added from an external source, CSP in this case, lifting the temperature to state 6 where the fluid enters the turbine. The fluid is expanded to state 7, producing work, and then directed into the HTR (7 – 8) and LTR (8 – 9) to reject heat. The fluid at state 9 splits into the cooler and the auxiliary compressor where a percentage of the fluid is pressurised to the cycle's highest operating pressure. The remainder of the fluid is directed to the cooler (heat rejection unit), where it is cooled to targeted CIT (state 1) before returning to the main compressor.[14]

3.2. sCO_2 BRC heat rejection unit

The heat rejection unit is an essential part of any cyclic heat engine whose role is to ensure effective energy transfer from the heat engine to the surrounding. According to Carnot, operating the heat rejection unit at low temperatures may contribute to enhancing to the overall power cycle's efficiency. Considering the above, a prior investigation was conducted to advise on the operating temperature of the sCO_2. This investigation took foundation from Ehsan [10], revealed that the sCO_2 BRC has the potential to achieve greater efficiencies for higher overall pressure ratios, around 2.5, for CITs ranging between 30 – 35 °C as showed in fig. 3 below. Therefore, 32 °C is used as targeted CIT for the heat rejection unit.

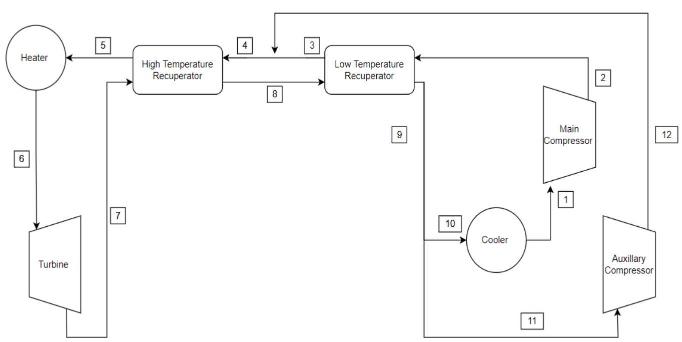

Fig. 2. Brayton Recompression Cycle Layout. [14]

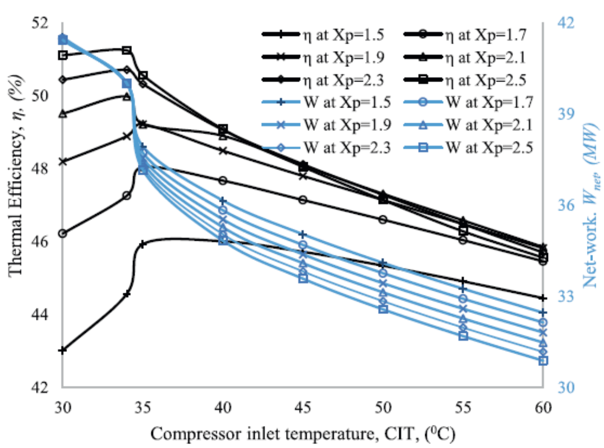

Fig. 3. s-CO_2 BRC efficiency and net power as function of pressure ratio CIT. [10]

To determine the heat rejection cooling capacity, a Flownex simulation model of a 20 MW sCO_2 BRC was built and simulated by Tshamala *et al.* [12] using 32 °C as CIT. This simulation revealed that to maintain a constant 32 °C CIT in an environment affected by daily variations in DNI, the heat rejection unit should be able to effectively transfer 20.36 MW of heat. Thus, this cooling duty together with the heat rejection unit inlet temperatures and the CIT are therefore used to advise the design of the heat rejection unit heat exchanger.

3.3. sCO_2 BRC Shell-and-tube heat exchanger design considerations

3.3.1.STHE physical configuration

The current shell-and-tube heat exchanger (STHE) was sized using the approach prescribed in the Tubular Exchanger Manufacturers Association (TEMA) standards [15]. This approach is used to ensure compliance with best practices and safety regulations. Hence, based on TEMA standards, the STHE design specifications such as shell type, tubes bundle type, tubes layout, tubes material, baffles type, spacing and cut, front-end head type, and rear-end type were selected as presented in Table 1. The above assisted to define to SHTE physical configuration. Choices resulting in the STHE physical layout are generally made with respect to specific criteria such as pressure requirements, cleaning method, cost of production, etc. However, for the purpose of the current STHE design, to maintain the carbon dioxide in supercritical region, the current design suggested to use 7.45 MPa as cycle's lowest pressure [14]. This value has been arbitrary chosen to ensure that at all time, the carbon dioxide remain in supercritical conditions, and not too high to ensure relatively effective gas expansion in turbine. This value will therefore be accounted for when selecting the tube size and thickness.

Table 1. Selected heat exchanger [15]

Front-end Head:	B-type
Shell Type:	E-type
Rear-end Head:	S-type
Tube Bundle Type:	Floating head type
Baffle Type:	Single segmental baffle
Baffle Cut:	25%
Baffle Spacing:	40% of the shell diameter
Tube Fluid:	sCO_2
Shell Fluid:	H_2O
Tube Layout:	30°
Tube Material:	Copper

3.3.2.STHE design methodology

At this stage of the design process, the required cooling duty, the operating pressure of the STHE, the sCO_2 inlet temperature to the STHE, and mass flowrate have been approximated based on thermodynamic cycle analysis; the cooling water inlet temperature approximated to ambient wet bulb temperature, since we operate on the assumption that a wet cooling tower is used to refresh the cooling water. The desired sCO_2 outlet temperature known (set to 32°C), and the sCO2 inlet temperature was set as 120°C which is the highest value established in Tshamala *et al.* [12]. The mass flowrate of the cooling water can be estimated using equations from basic heat transfer. The above assumed maximum 7 °C temperature difference between the inlet and the outlet temperature of the cooling water across the STHE [16]. Although both the e-NTU procedure as well as a LMTD method could be used for the sizing of the current STHE, for simplicity a decision for made to use only the LMTD method for sizing of the STHE. The above was done using equation (1) to define the overall heat transfer area.

$$Q = UA_oF\,\Delta T_{lm} \qquad (1)$$

In the above equation (1), Q, U, A, F, and ΔT_{lm} represent the cooling duty, the overall heat transfer coefficient, the total heat transfer area, the temperature correction factor, and the mean log temperature difference across the STHE. Equation (2) was used to evaluate the temperature correction factor introduced in equation (1).

$$F = \frac{\left(\sqrt{R^2+1}\right)\,\ln\left(\frac{1-S}{1-RS}\right)}{(R-1)\,\ln\left[\frac{2-S\left(R+1-\sqrt{R^2+1}\right)}{2-S\left(R+1+\sqrt{R^2+1}\right)}\right]} \qquad (2)$$

Where S is a measure of the temperature efficiency of the heat exchanger, and R is the thermal capacities ratio between the shell side and the tube side; calculated as below:

$$R = \frac{T_{CO2in} - T_{CO2out}}{T_{wout} - T_{win}} \quad (3) \quad \text{and} \quad S = \frac{T_{wout} - T_{win}}{T_{CO2in} - T_{win}} \quad (4)$$

With T_{win}, T_{wout}, T_{sCO2in} and $T_{sCO2out}$ representing the water inlet, water outlet, sCO_2 inlet and sCO_2 outlet temperatures respectively [17]. The ΔT_{lm} was obtained from the temperatures given above, while U, was estimated using an iterative approach. At first, both the shell-side and the tube-side heat transfer coefficients (h_w and h_{sCO2}) are guessed as 5000 W/m^{2}K on shell-side (water) and 500 W/m^{2}K (gas) on the tube-side [18]; using in conjunction equations (5) and (1), the heat transfer area A_o is obtained. In equation 3, the fouling resistances for both make-up water and sCO_2 were approximated by Kakac et *al.* [18]. To define the tubes configuration, equations (6) and (7) were used to determine the number of tubes (N_T) as well as shell diameter (D_s) of the STHE.

$$U_{fc}^{-1} = \frac{1}{h_w} + R_{fs} + \frac{d_o}{2\,k}\,\ln\left(\frac{d_o}{d_i}\right) + R_{ft} + \frac{PR}{h_{CO2}} \qquad (5)$$

In equation 5, R_{fs}, R_{ft}, k, d_i, d_o and PR are the shell-side fouling factor, the tube-side fouling factor, tube material thermal conductivity, the tubes inside diameter, tubes outside diameter and representing tube outside to inside diameter ratio.

$$D_s = 0.637\,\sqrt{\frac{CL}{CTP}}\,\left[\frac{A_f\,SO\,PR^2\,d_o}{L_T}\right]^{1/2} \qquad (6)$$

$$N_t = \text{round}\left[0.785\,\frac{CTP}{CL}\,\frac{{D_s}^2}{(PR\,d_o)^2}\right] \qquad (7)$$

Where CL represents the tube layout constant; CTP, the tube count calculation constant; L_T, the tubes active length, SO surface overdesign, and A_f, the heat transfer areas. [18]

According to literature, the optimum ratio between the tubes length and the shell diameter should be kept between 5 – 10, since it is a trade-off between the pressure drop on the shell side and manufacturing costs [18]. Engineering Equation Solver (EES) was used solve simultaneously all equations described in the model for variety of tube diameter. For each tube diameter, a parametric study was conducted to determine the corresponding tube length that would balance the heat transfer equation between the tube and shell sides of the STHE. The result of the parametric study is presented in Fig. 4 and Fig. 5, for only four diameters; hence for the purpose of this project a conservative approach suggested that a length-to-shell diameter of 5.31, using 22.225 mm tube outside diameter.[19]

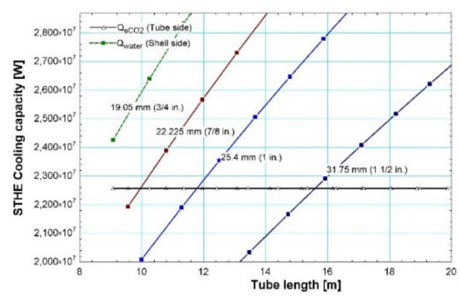

Fig. 4. STHE cooling capacity vs tube length for various tube diameters.

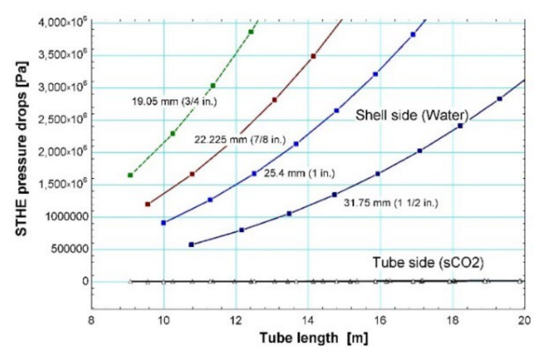

Fig. 5. STHE pressure drops vs tube length for various tube diameters.

In Fig. 4 above, the tube side heat transfer was found using the enthalpy change of sCO_2 between the inlet and the outlet of the STHE, while the shell side heat exchanger was found using equation 1. The shell side heat transfer coefficient was obtained using equation 8, while equation 10 approximated the tube side heat transfer coefficient. [18]

$$\frac{h_w D_e}{k_{mw}} = 0.36 \left[\frac{D_e\, G_w}{\mu_{mw}}\right]^{0.55} \left[\frac{cp_{mw}\, \mu_{mw}}{k_{mw}}\right]^{1/3} \left[\frac{\mu_{mw}}{\mu_w}\right]^{0.14} \qquad (8)$$

$$D_e = \frac{4\left(\frac{P_T^{\,2}\sqrt{3}}{4} - \frac{\pi\, d_o^{\,2}}{8}\right)}{\frac{\pi\, d_o}{2}} \qquad (9)$$

$$h_{sCO2} = \frac{k_{sCO2}}{d_i}\left[\frac{\frac{f_D}{8}\left(Re_{sCO2} - 1000\right) Pr_{sCO2}\left[1 + \left(\frac{d_i}{L_T}\right)^{0.67}\right]}{1 + 12.7\left(\frac{f_D}{8}\right)^{0.5}\left(Pr_{sCO2}^{\;0.67} - 1\right)}\right] \qquad (10)$$

Where:

$$f_D = [0.79\ \ln(Re_{sCO2}) - 1.64]^{-2} \qquad (11)$$

In equation 8, D_e is the hydraulic diameter applicable on the shell side for triangular tube configuration, G_w is the water mass flux; cp_{mw}, k_{mw}, and μ_{mw} are the water specific heat, thermal conductivity, kinematic viscosity expressed at mean temperature respectively, μ_w the water kinematic viscosity at well temperature. And in equation 10, f_D represents the friction factor on the tube side; Re_{sCO2}, Pr_{sCO2}, and k_{sCO2} are the Reynolds number, the Prandtl number, and the thermal conductivity of sCO_2, respectively. Hence, the results of the above approximation converged to 416.2 W/m^2K on the tube-side (h_{sCO2}) and 10307 W/m^2K on the shell-side (h_w). The subscript m in the thermophysical properties refers to the thermophysical properties evaluated at mean temperature, while w refers to water. Although tube side pressure drops were not described as one of the driving factors of decision for STHE sizing, it was found necessary to estimate them and present them in Fig. 6 below (Tube side of Fig.5 enhanced).

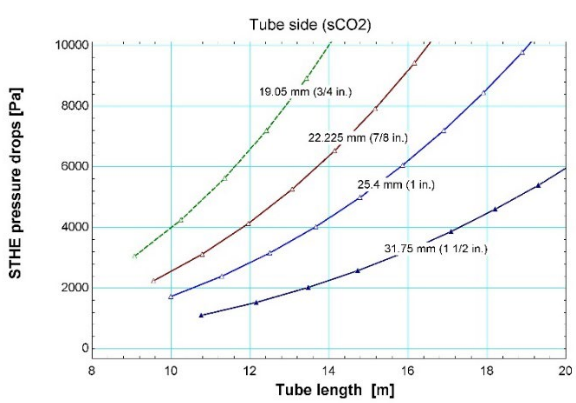

Fig. 6. STHE tube side pressure drops vs tube length for various tube diameters.

From Fig 5 and Fig. 6, it could be seen that at 22.225 mm tube outside diameter and 9.95 m tube length, the corresponding pressure drops on the shell side and the tube are 1.4 MPa and 2.5 kPa.

For the rating of the designed STHE, five methods were investigated, including the traditional e-NTU, the Kern, the Taborek, the Bell, and the Bell Delaware. It was found that although the first four could approximate the heat transfer coefficient and pressure drops with reasonable accuracy, the Bell Delaware method considers most of the fluid complexities as the fluid passes for baffle to tubes and vice versa, hence was found to be the most accurate. [20]

3.3.3.STHE rating – The Bell Delaware method

This method suggests that the designer initially start by estimating the tube size, the tube length, the heat transfer coefficient, the baffle spacing as well as the pitch ratio. Using an iterative approach, the pressure drops as well as the heat transfer coefficient was computed iteratively to convergence for the shell side fluid flow as well as the tube side fluid flow with the equations listed in Table 2. This process was repeated for a variety of tube sizes and lengths to approximate the appropriate heat exchanger dimensions.

Table 2. Pressure drop and heat transfer equations [18]

Shell Side (Water)	
Pressure drops:	$\Delta P_s = \frac{f_s\, G_w^{\,2}\, D_s\,(N_b+1)}{2\,\rho_{mw}\, D_e\, \Phi_s}$ (12)
Heat transfer coefficient:	$h_B = h_{id}\, J_c\, J_l\, J_b\, J_s\, J_r$ (13) Where: $h_{id} = J_i\, cp_{mw}\, G_w \left[\frac{k_{mw}}{cp_{mw}\mu_{mw}}\right]^{2/3} \Phi_s$ (14)
Tube side (sCO_2)	
Pressure drops:	$\Delta P_{ft} = \left[\frac{4\, f_D\, N_P\, L_T}{d_i} + 4\, N_P\right] \frac{G_{CO2}^{\;2}}{2\,\rho_{mCO2}}$ (15)
Heat transfer coefficient	Use equations 10 and 11

In table 2, f_s, N_b, Φ_s, ρ_{mw}, N_P, G_{CO2}, and ρ_{mCO2} are shell-side friction factor, number of baffles, water density at mean temperature, number of tube passes, carbon dioxide mass flux, and carbon dioxide mean density. J_i, J_c, J_l, J_b, J_s, and J_r are the corresponding correction factors for Colburn j-factor, baffle cut and spacing, baffle leakage, baffle spacing at inlet/outlet, bundle bypassing and Reynolds number correction.

4. Sensitivity analysis and cycle simulation

This simulation was done in Flownex. It was also important to determine whether the designed heat exchanger could maintain the temperature in the specified range. Table 3 presents overall cycle performance for CIT of 32 °C which is within the recommended target and 35 °C which aligned with the model verification discussed in the previous project [12].

Table 3 values were obtained through steady state simulation of the sCO_2 BRC assuming CIT at 35°C and at 32°C, for 10.4 MW and 20 MW net power. Table 3 values were obtained through steady state simulation of the sCO_2 BRC assuming CIT at 35°C and at 32°C, for 10.4 MW and 20 MW net power. Hence, to run the dynamic simulation of the complete cycle, it was necessary to integrate the designed STHE to the steady state model and implement variations in the solar DNI, ambient air temperature and wet bulb temperature.

Table 3. s-CO_2 BRC simulation model results

Targeted CIT [°C] / Plant size [MW]	35 / 10.4	35 / 20	32 / 20
MC Power [MW]	1.87	3.61	3.27
AC Power [MW]	2.31	4.44	4.35
Turbine Power [MW]	14.59	28.05	27.57
Net Power [MW]	10.44	20.00	19.87
Heat input [MW]	21.78	41.88	40.23
Efficiency [%]	47.76	47.77	49.4
Cooling Duty [MW]	11.34	21.88	20.36

The solar DNI was obtained from SOLARGIS, while the ambient air temperature as well as wet bulb temperature were sourced from the South African weather services for a typical hot day of the year 2022.

At this stage, it is necessary to specify that the sizing discussed in section 3 allowed to determine all other dimensions of the STHE as shown in Table 4. Information provided in Table 4 are used to build the STHE in Flownex, and the STHE simulation model was integrated in the sCO_2 BRC to close the loop and finally enabling the overall cycle dynamic response analysis.

Table 4. STHE design characteristics

Tube Outer Diameter (d_o)	mm	22.225
Tube pitch ratio (PR)	-	1.25
Tube Inner Diameter (d_i)	mm	17.78
Tube Length (L_T)	m	16
Tube Pitch (P_T)	mm	27.78
Baffle Cut (BC)	%	25
Number of Tubes (N_T)	-	4258
Shell Diameter (D_S)	m	2

5. Results and discussion

Two scenarios were investigated. The first being the ideal scenario where the heat input to the cycle was constant and secondly the heat input to the cycle was allowed to track the daily variation of the DNI. The 20 MW net power solarized sCO_2 BRC was designed using a solar field capable of supplying 44 MW thermal as peak capacity while for the second simulation, the cycle heat addition was simulated using the DNI and ambient temperature daily profiles. In both cases, the cooling water mass flow rate is maintained constant, and its temperature was approximated to the daily variation of the wet bulb temperature in the Upington. According to Uvarov *et al.* [21], knowing the ambient temperature, one could approximate the wet bulb temperature; however, for the current simulation this temperature was measured and supplied by the SAWS. A varying ambient temperature for a typical hot day in Upington, March 10th, 2022, was used. The results of both simulations are shown and discussed in the next few paragraphs.

With the first scenario (Figure 5 and 6), it can be observed that the heat exchanger can deliver a CIT ranging within the recommended values. The produced net power and the cycle efficiency are close to the predicted steady state values, 20.7 MW and 46% for mass flow rate approaching the designed maximum mass flow rate for the turbine used. The sCO_2 mass flow distribution between the two compressors depends on the split ratio (SR), which is the ratio of the secondary compressor mass flow to the total mass flow in the turbine. For this case, the SR fluctuates at about 30%. Regardless of the wet bulb temperature hourly variations, the CIT was effectively maintained to a maximum of 31.6 °C, which is well below the 35 °C where sCO_2 properties become unstable.

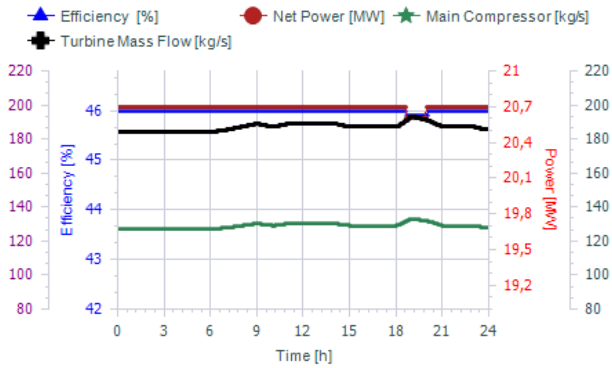

Fig. 5. Cycle efficiency, Net power, Main compressor mass flow, and turbine mass flow for constant heat load

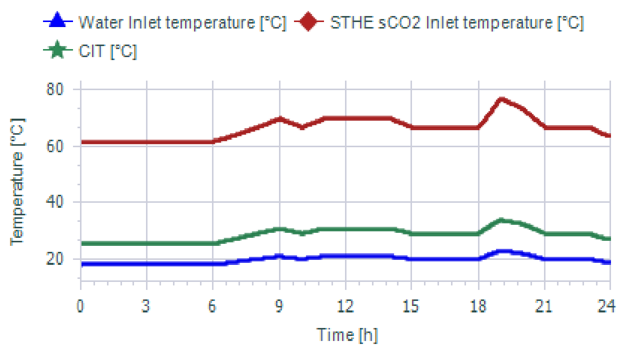

Fig. 6. CIT, Cooling water inlet temperature and STHE sCO_2 inlet temperature for constant heat load

The efficiency curve of the original cycle with the CIT of 35 °C is shown in Figure 7. This graph shows that at 35 °C CIT, the efficiency was recorded as 45.6% regardless of the DNI variation (Heat input). This efficiency slightly increased to about 46% when the CIT drops to 31.6 °C. according to literature, the efficiency is expected to be at its best value at 33 °C. [10]

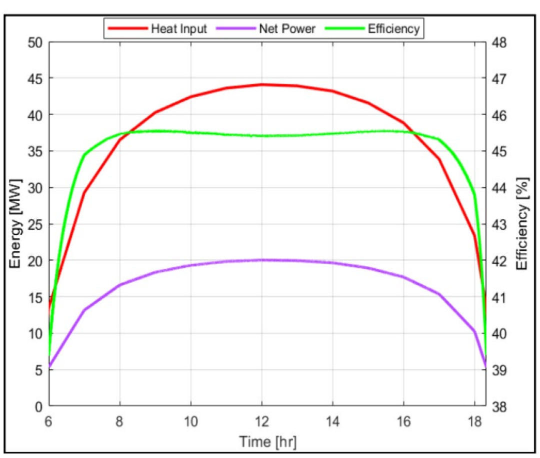

Fig. 7. Heat input, Net power, Efficiency for 35°C CIT cycle [12]**.**

However, in the study of efficiency increase, two other parameters are critical to ensure best values. Figure 8, discussed by Ehsan [10] shows that there is a strong correlation between the split ratio with the cycle thermal efficiency, which was not part of the current investigation. Hence, it is believed that pressure ratio and split ratio may play a significant role for the efficiency improvement to achieve performances predicted in Ehsan [10] as it can be seen in Figure 8.

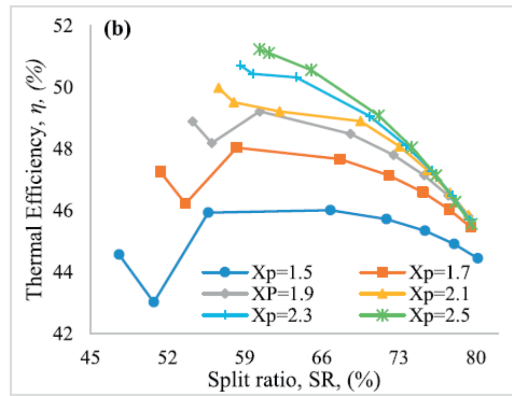

Fig. 8. Thermal efficiency variation with split ratio and pressure ratio of a sCO_2 BRC [10]

The second scenario, the full dynamic simulation of the sCO2 BRC power block with STHE integrated to the loop, was performed using input variables presented in Figure 9. The ambient temperature and the DNI were used to estimate the heat input to the system, while the wet bulb temperature is used as input at the STHE, representing the heat rejection unit.

Figure 10 is a display of the full cycle response to variation in weather conditions and solar energy. The efficiency still starts at 6am at 47% but slightly decreases to 46% when the full heat input is applied, then rises again as the heat input decreases. Many reasons could be responsible for the observed changes, since operating with many variables. However, the heat input variations can be highlighted as one of the many reasons. As the heat input increases, the turbine inlet temperature (TIT) in figure 11 tends to rise, however, the inventory control system constantly attempts to maintain the TIT at 700 °C by adjusting the total mass flow through the turbine. The above is believed to be the main reason for severe fluctuations observed in the TIT as well as the efficiency from around 13h00 through the after until sunset as shown in figure 11.

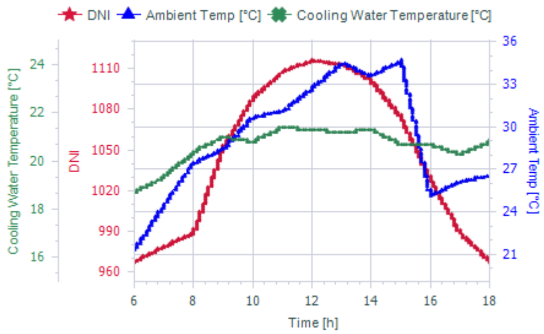

Fig. 9. Upington selected DNI, ambient temperature and wet bulb temperature [22] [4]

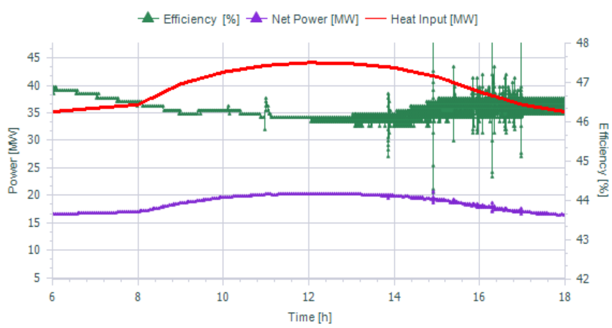

Fig. 10. sCO_2 BRC cycle efficiency and net power for variable heat load

In figure 10, the heat input is observed to rise as the day progresses in the morning times and decreases progressively in the afternoon. With it, the net power of the cycle increases to reach the power block's rated capacity when the heat input reaches it maximum. On the heat rejection site, it can be observed in figure 12 that the cooling load also follows the heat input trend, with a little deviation due to ambient conditions changes.

Another important observation is made on the CIT which starts just about 26 °C (compressed liquid), then increases, reaching its maximum when the heat input reaches its maximum, then decreases progressively in the afternoon. The above is due to a combined effect of the variation of the sCO_2 mass flow in the cycle induced by the inventory control system, the low wet bulb temperature early in the day and late in the afternoon, as well as the unchanged mass flow of the cooling water through the STHE for the duration of the simulations. Figure 11 also shows the STHE sCO_2 inlet temperature, which changes because of feedback introduced by the STHE in the cycle.

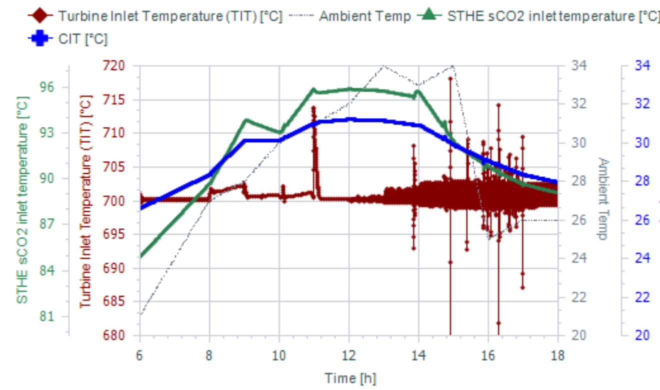

.

Fig. 11. Turbine inlet temperature, CIT, STHE sCO_2 inlet temperature and ambient temperature fluctuations for variable heat load.

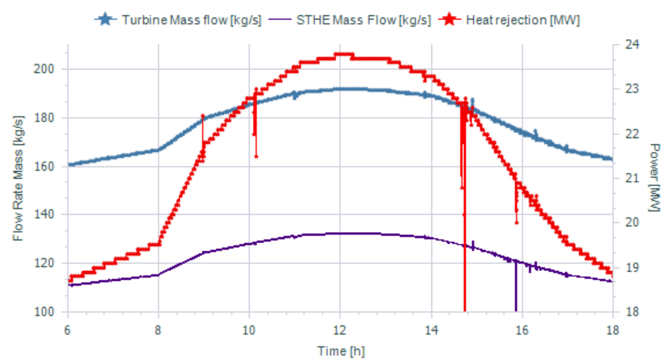

Fig. 12. STHE cooling load, mass flow through the turbine and main compressor variation for variable heat load.

6. Conclusion

The aim of this project was to design a STHE with capacity to service a sCO_2 BRC powered by CSP, then investigate the overall cycle dynamic response to variable heat input as well as ambient temperatures. A water cooled STHE was designed using the traditional mean-log temperature difference approach during the first iteration sizing, which was enhanced using the Kern approach to refine the optimum dimensions, and Bell-Delaware considered for rating. Industry recommendations were used to make final decisions on the STHE design parameters accounting for the balance between manufacturing cost and pressure losses. The designed heat exchanger was then used in a simulation of a sCO_2 BRC at both constant heat load as well as variable heat load. The simulation results of the sCO_2 BRC have shown that the designed STHE adequately performed, maintaining the CIT below 32 °C, however the efficiency remained lower than the targeted 52%. The above revealed that decreasing the CIT alone is necessary to enhance the stability of the power cycle, however other aspects such the pressure ratio and split ratio are critical to further improve the overall cycle efficiency.

Acknowledgements

Authors would like to acknowledge the support received from the Solar Thermal Research Group (STERG) and the Centre for Renewable and Sustainable Energy Studies (CRSES) for the funding and administration support which enabled the authors to present the findings of this study at the Southern African Sustainable Energy Conference (SASEC 2023). These acknowledgements are also extended to the Mechanical and Mechatronic department staff for their support and guidance.

References

[1] I. E. Agency, "World Energy Outlook," 2022.

[2] S. G. Mantashe, "Integrated Resource Plan," 2019.

[3] T. Cebecauer, A. Skoczek, J. Betak, and M. Suri, "Site Assessment of Solar Resource Upington Solar Park," 2011.

[4] SAwS, "Annual State of the Climate of South Africa 2020," *Annu. State Clim. South Africa 2020*, vol. 1, no. 1, p. 30, 2021, [Online]. Available: https://www.weathersa.co.za/Documents/Corporate/Annual State of the Climate 2019.pdf.

[5] V. T. Cheang, R. A. Hedderwick, and C. McGregor, "Benchmarking supercritical carbon dioxide cycles against steam Rankine cycles for Concentrated Solar Power," *Sol. Energy*, vol. 113, pp. 199–211, 2015, doi: 10.1016/j.solener.2014.12.016.

[6] Y. A. Cengel, M. A. Boles, and M. Kanoglu, *Thermodynamics: An Engineering Approach*, 9th Editio. Mc Graw Hill Education, 2019.

[7] V. Dostal, P. Hejzlar, and M. J. Driscoll, "High-performance supercritical carbon dioxide cycle for next-generation nuclear reactors," *Nucl. Technol.*, vol. 154, no. 3, pp. 265–282, 2006, doi: 10.13182/NT154-265.

[8] A. Yu, W. Su, X. Lin, and N. Zhou, "Recent trends of supercritical CO2 Brayton cycle: Bibliometric analysis and research review," *Nucl. Eng. Technol.*, vol. 53, no. 3, pp. 699–714, 2021, doi: 10.1016/j.net.2020.08.005.

[9] P. Jiang, B. Wang, Y. Tian, X. Xu, and L. Zhao, "Design of a Supercritical CO2Compressor for Use in a 1 MWe Power Cycle," *ACS Omega*, vol. 6, no. 49, pp. 33769–33778, 2021, doi: 10.1021/acsomega.1c05023.

[10] M. M. Ehsan, S. Duniam, J. Li, Z. Guan, H. Gurgenci, and A. Klimenko, "Effect of cooling system design on the performance of the recompression CO2 cycle for concentrated solar power application," *Energy*, vol. 180, pp. 480–494, 2019, doi: 10.1016/j.energy.2019.05.108.

[11] G. B. Eke and C. A. Ebieto, "Performance Analysis of Shell and Tube Heat Exchangers : A case study," *J. Emerg. Trends Eng. Appl. Sci.*, vol. 3, no. 5, pp. 899–903, 2012.

[12] M. C. Tshamala, C. Govender, T. M. Hans, C. McGregor, and M. T. F. Owen, "Thermodynamic Analysis of a 20 MW Concentrated Solar-Powered Supercritical Carbon Dioxide Brayton Recompression Cycle," Proceedings of the 16th International Conference on Heat Transfer, Fluid Mechanics and Thermodynamics HEFAT-ATE 2022, pp. 984–995.

[13] M. T. White, G. Bianchi, L. Chai, S. A. Tassou, and A. I. Sayma, "Review of supercritical CO2 technologies and systems for power generation," *Appl. Therm. Eng.*, vol. 185, no. November 2020, 2021, doi: 10.1016/j.applthermaleng.2020.116447.

[14] K. Brun, P. Friedman, and R. Dennis, *Fundamentals and applications of supercritical carbon dioxide (sCO2) based power cycles*, 1st Editio. Woodhead Publishing, 2017.

[15] R. C. Byrne, "TEMA Standards of the Tubular Exchanger," 2019.

[16] P. Roy, I. N. Rao, T. R. Martha, and K. V. Kumar, "Discharge water temperature assessment of thermal power plant using remote sensing techniques," *Energy Geosci.*, vol. 3, no. 2, pp. 172–181, 2022, doi: 10.1016/j.engeos.2021.06.006.

[17] G. Towler and R. Sinnott, *Chemical Engineering Design Principles , Practice and Economics of Plant and Process Design Second Edition*. .

[18] S. Kakaç, H. Liu, and A. Pramuanjaroenkij, *HEAT EXCHANGERS: Selection, Rating and Thermal Design*. 2012.

[19] G. Towler and R. Sinnott, *Chemical Engineering Design: Principles, Practice and Economics of Plant and Process Design, Second Edition*. 2012.

[20] S. Y. Kulkarni, S. B. Jagadish, and M. B. Manjunath, "Analysis Comparing Performance of a Conventional Shell and Tube Heat Exchanger Using Kern, Bell and Bell Delaware Method," *Int. J. Res. Eng. Technol.*, vol. 03, no. 15, pp. 486–496, 2014, doi: 10.15623/ijret.2014.0315093.

[21] A. V. Uvarov, N. A. Sakharova, and N. A. Vinnichenko, "Effect of natural convection on the current-voltage characteristic of a DC discharge in neon at intermediate pressures," *Plasma Phys. Reports*, vol. 37, no. 12, pp. 1046–1052, 2011, doi: 10.1134/S1063780X11110092.

[22] Weatherspark, "Weather history at Upington Airport," 2022. https://weatherspark.com/h/d/148468/2022/1/22/Historical-Weather-on-Saturday-January-22-2022-at-Upington-Airport-South-Africa#Figures-Temperature (accessed May 04, 2023).